Size dependence of the optical spectrum in nanocrystalline silver

Praveen Taneja* and Pushan Ayyub†
Department of Condensed Matter Physics and Materials Science, Tata Institute of Fundamental Research, Homi Bhabha Road, Mumbai 400005, India

Ramesh Chandra
Department of Physics, Guru Nanak Dev University, Amritsar-143005, India
(Received 8 October 2001; revised manuscript received 29 January 2002; published 29 May 2002)

We report a detailed study of the optical reflectance in sputter-deposited, nanocrystalline silver thin films in order to understand the marked changes in color that occur with decreasing particle size. In particular, samples with an average particle size in the 20 to 35 nm range are golden yellow, while those with a size smaller than 15 nm are black. We simulate the size dependence of the observed reflection spectra by incorporating Mie's theory of scattering and absorption of light in small particles, into the bulk dielectric constant formalism given by Ehrenreich and Philipp [Phys. Rev. **128**, 1622 (1962)]. This provides a general method for understanding the reflected color of a dense collection of nanoparticles, such as in a nanocrystalline thin film. A deviation from Mie's theory is observed due to strong interparticle interactions.

DOI: 10.1103/PhysRevB.65.245412 PACS number(s): 78.67.Bf, 73.21.−b, 81.15.Cd

I. INTRODUCTION

The optical properties of nanometer-sized metal particles have been of both experimental and theoretical interest for some time. It has been known for over a thousand years that the color of small metal particles embedded in glass depends strongly on the size and shape of the particles. The optical properties of such colloidal systems are ascribed to surface plasmon resonance caused by the incident light. The characteristics of the resulting absorption bands can be calculated from the well-known Mie theory.[1–3] The peak position as well as linewidth of the surface plasmon depend on the particle size. Strong quantum size effects are observed when the linear dimension of a particle is smaller than the electronic mean free path in the corresponding bulk material.[4–7] However, most of the existing experimental and theoretical work refers to dilute dispersions of metallic nanoparticles in media such as air, liquids, or dielectric matrices. The optical extinction spectra of silver particles in the form of free or embedded clusters[8–10] in a dielectric matrix, submicrometer-size needles,[11] microlithographically produced silver spheres,[12] etc. have been studied. Generally, a peak is observed in the optical absorption spectrum, and is interpreted as the surface plasmon (SP) absorption predicted by Mie's theory. The width and position of surface plasmon not only depend on particle size as suggested earlier,[13] but also on the chemical properties of the nanocrystalline surface, referred to as chemical interface damping.[10] Reflectance studies on thick, nanocrystalline, opaque films have rarely been done[14,15] and no attempt to simulate the complete reflection spectrum has been made, though the deficit in the reflection due to SP absorption has been calculated using the quantum-mechanical probability that an incident photon will excite a surface plasmon.[15]

In recent years, the production and study of nanocrystalline thin films have assumed increasing importance. In this paper, we report the study of the optical properties of nanocrystalline silver thin films and attempt to explain the particle size induced changes in the color in terms of existing models. Specifically, we derive an expression that simulates the entire reflectivity spectrum covering the region where silver shows free-electron-like behavior as well as the regime where *d*-band electrons are excited to the conduction band, while also considering the effect of the SP absorption. The agreement with experimental spectra of samples with different particle size is quite satisfactory.

Since the electronic configuration of a silver atom is $[Kr]4d^{10}5s^1$, the outermost $(5s)$ energy band is only half filled, which is why silver is a metal. However, the immediately underlying *d*-band electrons affect the optical and electronic properties much more markedly in silver than in copper or gold. The reflectivity of bulk silver is almost independent of wavelength and close to 100% over the entire visible region. It was first shown by Ehrenreich and Philipp[16] that this is a combined effect of the conduction-band electrons of the *s* band as well as the interband transitions from the *d* band to the conduction band.

As the average particle size in sputter-deposited nanocrystalline silver is reduced, we observe a marked change in its color, from white (in the bulk) to golden yellow to gray and finally to jet black, in particles smaller than 10 nm. We show that such a size dependence of the color in nanocrystalline thin films, can be explained on the basis of Mie's theory of absorption and scattering of light from small metal particles with a complex refractive index, combined with the bulk dielectric constant formulation given by Ehrenreich.

II. EXPERIMENTAL DETAILS

Nanocrystalline silver thin films were deposited using high-pressure dc-magnetron sputtering. The sputtering was carried out in a custom-built chamber using a 200 mm long, axial, planar magnetron source (Atom Tech 320-O). The sputtering target was a 99.99% pure silver disc (50 mm diameter), placed 55 mm away from the substrate. The base pressure was better than 1×10^{-6} Torr, while sputtering was

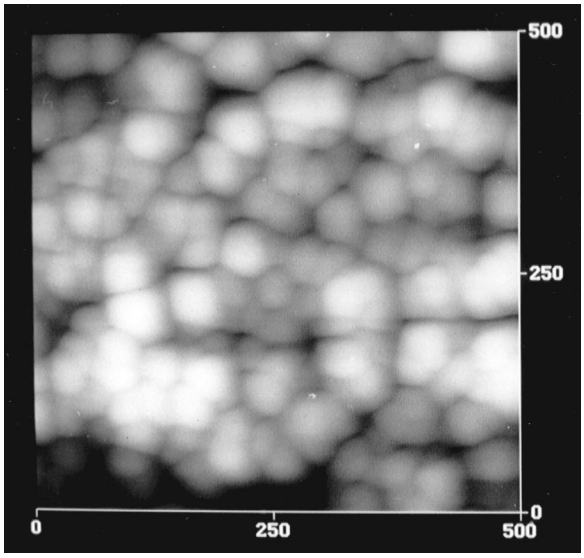

FIG. 1. Atomic force micrograph recorded for a 500 nm $\times$500 nm area of a typical nanocrystalline Ag film deposited at 100 K.

carried out in the presence of flowing Ar or He, at a pressure between 5 m Torr and 100 m Torr. At such relatively high pressures, the sputtered silver atoms lose much of their kinetic energy in colliding with the gas atoms and arrive at the substrate with little energy left for surface diffusion. The nanoparticles were deposited on quartz or glass substrates, maintained at either 273 K (cooled with ice water) or close to 100 K (cooled with liquid nitrogen). The nanocrystalline thin films typically consist of a collection of densely packed, approximately spherical, silver nanoparticles, deposited on a quartz substrate, as shown in the atomic force micrograph in Fig. 1. Both the high sputtering pressure and the low substrate temperature inhibit the growth of large particles. These two parameters, as well as the dc voltage applied to the target were used to control the particle size (see Table I). Further details of the sputtering process for silver nanoparticles are described elsewhere.[17,18]

The coherently diffracting crystallographic domain size (d_{XRD}) of the silver nanoparticles was calculated from x-ray diffraction (XRD) line broadening after subtracting the contribution from the CuKα_2 component (Rachinger correction) and correcting for the instrumental width. The integral linewidth was used in the Scherrer formula[19] to calculate d_{XRD}. Figure 2 shows the (111) reflection (used for calculating d_{XRD}) in the XRD spectra of bulk silver and sputter-deposited nanocrystalline thin films with different average sizes.

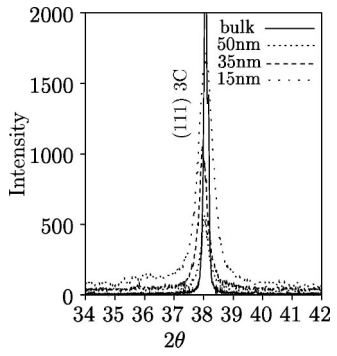

FIG. 2. X-ray diffraction pattern showing the (111) line of nanocrystalline silver with different average sizes.

The optical reflection and transmission from the nanocrystalline thin films were measured in the 200–900 nm range using a Shimadzu UV-2100 uv-visible spectrophotometer. The specular reflection was recorded with the incident angle being set to 8°, while the light scattered in 2π directions was recorded at normal incidence, using an integrating sphere. In the latter case, the specular part of the reflected light goes back to the source and the scattered light is collected by the integrating sphere internally coated with white powder such that all the scattered light reaches the photomultiplier tube after multiple reflections. The scattered light intensity was $\sim$5% of the incident intensity at large wavelengths in all the sputtered films, indicating that the surface smoothness of the films was very high at optical length scales.

The value of the transmitted intensity was close to zero throughout, except near 320 nm (plasma wavelength) where it was about 3–4 %. This is because the skin depth for bulk silver is nearly 10 nm in the visible range, while the film thickness was typically 500 nm. For wavelengths smaller than 320 nm the interband absorption becomes significant and the transmission again falls to zero. Since we do not observe any interference fringes in the reflection spectrum, we can safely neglect the transmission of light through the film for the purpose of theoretically fitting the data in the wavelength range of 320 to 800 nm.

III. RESULTS AND DISCUSSION

The true color photograph in Fig. 3 shows that there is a rather striking change in the color of sputter-deposited nanocrystalline silver with decreasing size. This picture was obtained from powder samples (with different average sizes) scraped off the substrate and dispersed on a glass slide. Clearly, the sample with the $d_{XRD}=50$ nm is silvery white,

TABLE I. Conditions for the sputter synthesis of nanocrystalline silver films with different particle sizes.

d_{XRD} (nm)	Pressure (Torr)	Applied voltage (V)	Substrate	Substrate temperature (K)
Bulk		Siver disk (99.99% pure)		
50	5.4×10^{-3}	280	Glass	100
35	1.1×10^{-1}	388	Quartz	298
15	8.0×10^{-2}	401	Glass	100

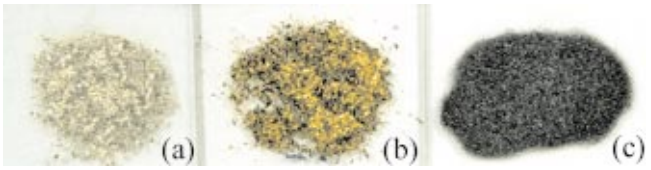

FIG. 3. (Color) True color photograph of nanocrystalline silver samples with different average x-ray sizes (d_{XRD}): (a) 50 nm, (b) 35 nm, and (c) 15 nm.

while the sample with $d_{XRD}=35$ nm is golden yellow. The color of this sample is stable and does not change when exposed to air for several months. Nanocrystalline silver with a particle size in the 20–35 nm range, therefore, appears to have a potential industrial application as a decorative coating. When the average size is reduced further, the color becomes gray and finally black.

Figure 4 shows the corresponding specular reflectance spectra of bulk silver and the three nanocrystalline silver films (with different average size), sputter deposited under the conditions given in Table I. We summarize below the salient features that emerge from a study of the size dependence of the reflectance spectra.

(1) The reflected intensity for the bulk sample is expectedly high ($\sim$90%) in the visible region of the spectrum. Due to plasma resonance, the reflectance falls sharply below $\sim$350 nm and reaches a minimum ($\sim$4%) at 320 nm. At even lower wavelengths, it rises again to $\sim$20% and remains constant till 250 nm.

(2) With a decrease in the particle size, the reflectance decreases at all wavelengths.

(3) The magnitude of the decrease in reflectance with particle size is itself a function of the wavelength, the decrease being larger at lower wavelengths.

(4) There is a well-defined dip in the reflection spectrum near $\lambda=360$ nm (marked as SPR in Fig. 4) due to surface plasmon resonance (SPR). This dip becomes increasingly prominent with decreasing particle size. The width of the dip also increases as the particle size gets reduced.

The nature of the observed color change with particle size (Fig. 3) can be correlated easily with the reflection spectra in Fig. 4. Obviously, bulk silver is white because the reflectance is very high in the entire visible region. With a decrease in the particle size, the spectrum gets depleted most in the blue end, relatively less in the green region, and the least in the red. This results in a golden-yellow color. At smaller sizes, the reflected intensity is quite low throughout the spectrum,

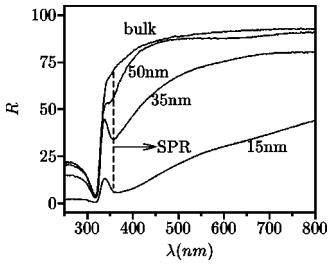

FIG. 4. Experimental reflectance spectrum of bulk silver and nanocrystalline silver films with different particle sizes (d_{XRD}).

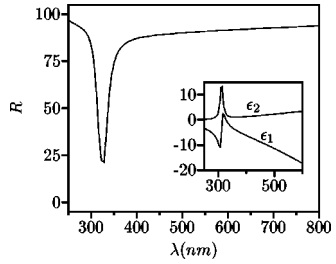

FIG. 5. Reflectance spectrum for bulk silver computed using Eq. (2). Inset shows the corresponding dielectric constant spectra.

leading to a color that is dark gray, and finally black.

We now show that the reflection spectra for different particle sizes can be quantitatively simulated on the basis of Mie's theory of scattering and absorption of light by small particles, combined with Ehrenreich's formulation[16] for the reflection spectrum for bulk silver. The reflectance spectrum for bulk silver can be obtained from the dielectric function, $\epsilon(\omega)$, which can be expressed as a sum of the free-electron contribution, $\epsilon_{free}(\omega)=4\pi J\sigma(\omega)/\omega$, and a bound-electron contribution, $\epsilon_{bound}(\omega)$. The ac conductivity, $\sigma(\omega)$, is given by $\omega_p^2/[4\pi(\gamma-J\omega)]$, where ω_p is the plasma resonance frequency, and γ is the free-electron damping coefficient. Finally, the reflectivity $R(\omega)$ can be expressed as

$$R(\omega)=100\times\left|\frac{1-\eta(\omega)}{1+\eta(\omega)}\right|^2, \tag{1}$$

where the refractive index $\eta(\omega)=\sqrt{\epsilon(\omega)}$.

In the case of silver, the free-electron plasma frequency lies at $\hbar\omega_p=9.2$ eV, but the onset of interband transitions occurs at $\hbar\omega_1=3.9$ eV. The contribution of $\epsilon_{bound}(\omega)$ to $\epsilon(\omega)$, makes the latter vanish at a lower value of energy ($\sim$3.9 eV), where it gives rise to a *hybrid* plasma resonance. In the simplest case, we can describe $\epsilon_{bound}(\omega)$ by a single frequency resonance at $\hbar\omega_1=3.9$ eV, with an oscillator strength f_1 and damping coefficient γ_1,

$$\epsilon_{bound}(\omega)=1+\frac{f_1\omega_{p1}^2}{\omega_1^2-\omega^2-J\omega\gamma_1}. \tag{2}$$

However, Eq. (2) does not correctly simulate the reflectance of *bulk* silver above 3.9 eV (below 319 nm) where the calculated reflectance rises rapidly to $\sim$90% (Fig. 5) while the observed reflectance in this region is only about 25% (Fig. 4). This is explained by the inset in Fig. 5, which shows the corresponding real (ϵ_1) and imaginary (ϵ_2) parts of the dielectric constant plotted as a function of wavelength. Clearly, Eq. (2) describes a single frequency resonance at $\hbar\omega_1=3.9$ eV. For frequencies larger than ω_1, the second term of $\epsilon_{bound}(\omega)$ in Eq. (2) becomes negative (the damping term $J\omega\gamma_1$ only broadens this change), thus making $\epsilon_1(\omega)$ even more negative, the contribution from $\epsilon_{free}(\omega)$ being already negative at and above 3.9 eV. This leads to an unrealistically large value of $\eta_2(\omega)$, and hence the reflectance $R(\omega)$, in this region.

In reality, $\hbar\omega=3.9$ eV only marks the onset of a *con-*

tinuum of transitions from the quasicontinuous electronic energy levels of the *d* band to those of the *s* band and beyond. The effect of this continuum of transitions, can be simulated by integrating $\epsilon_{bound}(\omega)$ with the transition frequencies ω_{1i} treated as a continuous variable. This requires a knowledge of the frequency dependence of the number density of interband transition frequencies ρ, as well as the frequency dependence of the oscillator strengths, $f_1(\omega)$, and the damping coefficients, $\gamma_1(\omega)$. For simplicity, we assume that these quantities are frequency independent in the range $\hbar\omega_1 = 3.9$ eV to $\hbar\omega_2 = 6.2$ eV, with ω_2 being an arbitrarily chosen upper bound for interband transitions. We can now analytically integrate the contribution of $\epsilon_{bound}(\omega)$ to $\epsilon(\omega)$ as follows:

$$\epsilon(\omega) = 1 - \frac{\omega_p^2}{\omega^2 + J\omega\gamma} + \rho\omega_{p1}^2 \int_{\omega_1}^{\omega_2} \frac{1}{\omega_1^2 - \omega^2 - J\omega\gamma_1} d\omega_1$$

$$= 1 - \frac{\omega_p^2}{\omega^2 + J\omega\gamma} + \rho\omega_{p1}^2 \left[\frac{\tanh^{-1}\left(\frac{\omega_1}{\sqrt{J\omega\gamma_1 + \omega^2}} \right) - \tanh^{-1}\left(\frac{\omega_2}{\sqrt{J\omega\gamma_1 + \omega^2}} \right)}{\sqrt{J\omega\gamma_1 + \omega^2}} \right]. \quad (3)$$

In Eq. (3) both ρ and ω_2 decide the extent of the contribution of $\epsilon_{bound}(\omega)$ to $\epsilon(\omega)$ and thus both parameters influence the position of the plasma reflectivity edge. Therefore only when an arbitrary value of ω_2 (somewhat greater than ω_1) has been fixed, can the value of ρ be determined. In our fitting we have chosen $\hbar\omega_2 = 6.2$ eV, which gives $\rho = 0.2658 \times 10^{-14}$ s. If the value of ω_2 is slightly increased, the fitted value of ρ slightly decreases to give the correct plasma reflectivity edge. So, our ignorance of the functional form of $f(\omega)$, $\rho(\omega)$, and the actual upper bound of interband transitions is hidden in the fitting parameter ρ.

The inset in Fig. 6 shows the real and imaginary parts of $\epsilon(\omega)$, as given by Eq. (3). In contrast to Fig. 5, $\epsilon_1(\omega)$ does not have a large, negative value at frequencies greater than ω_1. Also, $\epsilon_2(\omega)$ does not decay to zero. Figure 6 shows the fitting of $R(\omega)$ calculated using Eq. (3) to the reflectance data for bulk silver. Evidently, the integrated expression for $\epsilon_{bound}(\omega)$ leads to more realistic values of reflectivity in the short wavelength region of interband transitions. The fit should improve further when the actual ω dependence of the number density of interband transitions, oscillator strengths, and damping coefficients are incorporated. Note also that just above the sharp drop in reflectance (at 319 nm), the experimental spectrum dips below the calculated value in the region between 350 and 400 nm. This arises from a small contribution due to the surface plasmon absorption, which is observed even in bulk silver with a microscopically rough surface, unless it is electrolytically polished.[20]

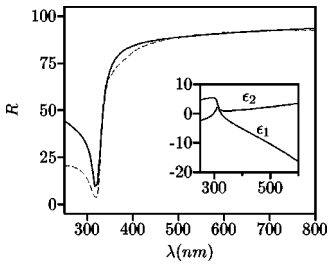

FIG. 6. Reflectance spectrum for bulk silver (continuous line) obtained using Eqs. (1) and (3), which take account of the contribution from the quasicontinuous interband transitions. The experimental reflectance spectrum is shown by a dashed line. Inset shows the corresponding dielectric constant spectra.

The expression for the reflectivity [Eq. (1)] is valid when light is incident on the planar interface between two *semi-infinite* media (described solely by their respective dielectric constants). However, as is clear from Fig. 1, the system under consideration is a densely packed ensemble of nearly spherical nanoparticles. We model this as a system that has partly bulklike properties (being densely packed, there is an overlap of wave functions between neighboring nanoparticles), and in part properties related to the confinement of individual nanoparticles. Therefore, even for the nanocrystalline film the reflectance spectra (Fig. 4) show some characteristic bulklike features (for example, the volume plasma frequency) in addition to surface plasmon effects arising from the bound spherical nature of individual nanoparticles. For the case in which the plane separating the two media is curved, as in a spherical nanoparticle in a dielectric medium, the solution is given by Mie's theory.[1] This describes the scattered and absorbed electric field amplitudes, when a plane electromagnetic wave is incident on a homogeneous sphere of arbitrary radius and dielectric constant. For an ensemble of spherical particles with a volume filling fraction q and radius a $(a \ll \lambda)$ embedded in a nonabsorbing-medium with dielectric constant ϵ_m, the extinction coefficient $K(\omega)$ is given by

$$K(\omega) = \frac{9\omega q}{c} \epsilon_m^{3/2} \frac{\epsilon_2(\omega)}{\{[2\epsilon_m + \epsilon_1(\omega)]^2 + \epsilon_2^2(\omega)\}}, \quad (4)$$

where, ϵ_1 and ϵ_2 are the real and imaginary parts of the bulk dielectric constant ϵ of the material that constitutes the spherical particles.

The frequency ω_s that minimizes the denominator of Eq. (4) leads to a maximum in the extinction spectrum, and is

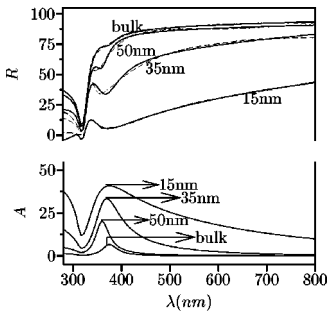

FIG. 7. Top, computed (solid line) and experimental (dashed line) reflectance spectra of nanocrystalline silver films with different particle sizes. The effect of surface plasmon absorption has been incorporated in this computation. Bottom, the corresponding surface plasmon absorption curves computed using Eq. (7).

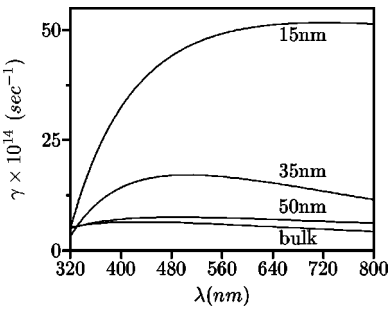

FIG. 8. Computed spectra for γas defined by Eq. (10) for different particle sizes.

known as the surface plasmon frequency. We now have Eq. (1) that, together with Eq. (3), explains the reflectivity of homogeneous (bulk) silver as well as Eq. (4) that gives the extinction coefficient of a SPR from the metallic nanoparticles embedded in a dielectric medium. We now show that the reflectivity spectrum of a nanocrystalline metallic thin film with an optically smooth surface can be simulated by simply subtracting the absorption of light due to SPR, from the bulk silver reflection. That is, $R_{nano}(\omega)$ is given by

$$R_{nano}(\omega)=R(\omega)-A_{SPR}(\omega), \tag{5}$$

where, the surface plasmon absorption, $A_{SPR}(\omega)$, is expressed as,

$$A_{SPR}(\omega)=100\{1-\exp[-K(\omega)t]\} \tag{6}$$

$$=100\left[1-\exp\left(\frac{-9\omega}{c}\epsilon_m^{3/2}\frac{\epsilon_2(\omega)}{\{[2\epsilon_m+\epsilon_1(\omega)]^2+\epsilon_2^2(\omega)\}}\delta\right)\right], \tag{7}$$

where, $\delta=t\times q$ is the effective penetration depth of light corrected for the filling fraction and is used as a fitting parameter.

The observed reflectivity spectra for opaque, nanocrystalline silver films with different average particle sizes are shown using broken lines in the upper half of Fig. 7. These data are fitted in the range $\lambda=320$ to 800 nm (solid curves) to the equations for $R_{nano}(\omega)$ [Eq. (5)], obtained after calculating $A_{SPR}(\omega)$ from Eq. (7), $R(\omega)$ from Eq. (1) and $\epsilon(\omega)$ from Eq. (3). The corresponding fitted SPR peaks are shown in the lower half of Fig. 7. Clearly both the width and the intensity of the SPR absorption increase with decreasing particle size, which leads to a frequency dependent decrease in the reflectance with a decrease in size. This is therefore directly responsible for the observed change in the color of nanocrystalline silver. In Eq. (7), the width of the resonance absorption is proportional to the damping coefficient γ appearing in $\epsilon_{free}(\omega)$. At sufficiently small sizes, additional damping of electrons is caused by the reduced particle size along with the usual defect scattering.[13] In fact, if v_f is the Fermi velocity then the scattering time constant τ_{surf} is given by

$$\tau_{surf}(a)=C\frac{a}{v_f}, \tag{8}$$

where, a is the radius of the particle and $C\simeq 1$. Since $\gamma=\tau^{-1}$,

$$\gamma_{nano}(a)=\gamma_{bulk}+\frac{v_f}{a}. \tag{9}$$

Thus the damping coefficient has an additional term that is inversely proportional to the particle size.

The least-square values of the fit parameters are given in Table II. Care was taken to redefine the variables such that all fitting parameters were nearly of the same order of magnitude. The fits improved markedly if we allowed the damping coefficient γ to have a frequency dependence of the form

$$\gamma(\omega)=a_1+a_2\omega+a_3\omega^2. \tag{10}$$

Figure 8 shows the frequency dependence of γ for different particle sizes. Clearly, as the particle size is reduced, γ increases substantially with increasing wavelength. The

TABLE II. Values of the fitting parameters used to calculate the reflectance spectra shown in Fig. 7, as defined in Eqs. (7) and (10).

d_{XRD} (nm)	ϵ_m	$\delta\times10^{-8}$ (m)	$a_1\times10^{14}$ (s^{-1})	a_2	$a_3\times10^{-14}$ (s)	$\sqrt{\frac{\chi^2}{N}}$ [a]
Bulk	1.97±0.02	0.0176±0.0005	−3.7±0.3	0.47±0.02	−0.0053±0.0002	1.02
50	1.520±0.006	0.078±0.001	−1.5±0.4	0.47±0.02	−0.0061±0.0002	1.13
35	1.885±0.008	0.191±0.002	−24.3±0.6	2.22±0.03	−0.0298±0.0004	1.59
15	2.574±0.008	0.4833±0.0009	22.3±0.7	2.25±0.04	−0.0432±0.0005	0.56

[a] χ^2 is the weighted sum of squared residuals and N represents the number of degrees of freedom.

width of the SP absorption is proportional to γ, which implies that for smaller particle sizes the absorption peak (for a fixed value of γ) is broader at longer wavelengths than what is given by Eq. (7). This deviation from Mie's extinction formula for a single particle has also been observed in colloidal aggregates of silver.[21] The extra broadening at longer wavelengths (which is reflected as an increase in the value of the wavelength-dependent γ in our derivation) has been explained on the basis of intercluster interactions. The silver aggregates are treated as fractals and it is assumed that the interaggregate interactions are dipole coupled to each other. The slight decrease of γ at longer wavelengths for larger particle sizes has also been reported earlier.[16] The γ vs λ plots for 15 nm and 35 nm appear to fall below the plots corresponding to the larger sizes (Fig. 8). This may simply be an artifact of the fitting accuracy (see Table II) in this region. Also, the contribution of the interband $(d \rightarrow s)$ transition has been included in a rather simplistic manner in the calculation of $\epsilon(\omega)$. Consequently, the values of all quantities calculated from $\epsilon(\omega)$ for wavelengths around and below 320 nm should not be expected to be very accurate, though the visible region of the spectrum is described properly.

We have also observed similar changes in color with particle size in the case of platinum and copper nanoparticles deposited by magnetron sputtering. Whereas bulk Pt is steel gray and Cu is orange, they are both completely black in the nanocrystalline form, when the particle size is less than ~ 10 nm. Nanocrystalline platinum—used as an electrocatalyst in fuel cell grade electrodes—is commercially known as platinum black.[22] Similarly, ''gold black''[23] is used as an infrared absorber. We may expect the physics involved in these cases to be similar.

IV. SUMMARY

We have prepared nanocrystalline silver thin films with different average particle sizes using high-pressure magnetron sputtering. With a reduction in the particle size, we observe a gradual change in the color of the nanocrystalline samples from white to golden yellow to gray and finally to jet black. The color of these nanoparticle samples can be understood on the basis of their measured reflectivity spectra. The experimental spectra are fitted to an expression derived from the assumption that the reflectance from an opaque, metallic, nanocrystalline thin film is equal to the reflectance from the bulk metal, minus the absorption due to surface plasmon resonance. This directly leads to a frequency dependent decrease in reflectance that explains the size dependence of the color of silver nanoparticles. The increase in the fitted value of the damping coefficient γ with a decrease in the particle size occurs because the mean scattering time of an electron is governed by the particle size in addition to collisions from defects. The increase in the value of γ at longer wavelengths for small particles indicates that the surface plasmon peak has an extra broadening in the long wavelength region. Our results extend the earlier observations in colloidal aggregates to more densely packed clusters in solid thin films.

ACKNOWLEDGMENTS

We thank Professor Mustansir Barma and Professor Nandini Trivedi for illuminating discussions and critically reading the manuscript. P. Taneja acknowledges partial support from the TIFR Endowment Fund.

*Electronic address: taneja@tifr.res.in
†Electronic address: pushan@tifr.res.in

[1] G. Mie, Ann. Physik. **25**, 377 (1908).
[2] V. Hulst, *Light Scattering by Small Particles* (Wiley, New York, 1957).
[3] G. F. Bertsch and R. A. Broglia, *Oscillations in Finite Quantum Systems* (Cambridge University Press, Cambridge, 1994).
[4] A. Kawabata and R. Kubo, J. Phys. Soc. Jpn. **21**, 1765 (1966).
[5] D. Wood and N. Ashcroft, Phys. Rev. B **25**, 6255 (1982).
[6] W. Halperin, Rev. Mod. Phys. **58**, 533 (1986).
[7] M. Barma and V. Subrahmanyam, J. Phys.: Condens. Matter **1**, 7681 (1989).
[8] S. Fedrigo, W. Harbich, and J. Buttet, Phys. Rev. B **47**, 10 706 (1993).
[9] B. Prevel, J. Lerme, M. Gaudry, E. Cottancin, M. Pellarin, M. Treilleux, P. Melinon, A. Perez, J. Vialle, and M. Broyer, Scr. Mater. **44**, 1235 (2001).
[10] H. Hovel, S. Fritz, A. Hilger, U. Kreibig, and M. Vollmer, Phys. Rev. B **48**, 18 178 (1993).
[11] M. Bloemer, T. Ferrell, M. Buncick, and R. Warmack, Phys. Rev. B **37**, 8015 (1988).
[12] B. Russel, J. Mantovani, V. Anderson, R. Warmack, and T. Ferrell, Phys. Rev. B **35**, 2151 (1987).
[13] U. Kreibig and C. Fragstein, Z. Phys. **224**, 307 (1969).
[14] M. Rasigni, G. Rasigni, J. Palmari, and A. Llebaria, Phys. Rev. B **23**, 527 (1981).
[15] J. Elson and R. Ritchie, Phys. Rev. B **4**, 4129 (1971).
[16] H. Ehrenreich and H. Philipp, Phys. Rev. **128**, 1622 (1962).
[17] R. Chandra, P. Taneja, J. John, P. Ayyub, G. Dey, and S. Kulshreshtha, Nanostruct. Mater. **11**, 1171 (1999).
[18] P. Ayyub, R. Chandra, P. Taneja, A. Sharma, and R. Pinto, Appl. Phys. A: Mater. Sci. Process. **73**, 67 (2001).
[19] B. Warren, *X-Ray Diffraction* (Addison-Wesley, Reading, MA, 1969).
[20] T. Huen, G. Irani, and F. Wooten, Appl. Opt. **10**, 552 (1971).
[21] V. Markel, V. Shalaev, E. Stechel, W. Kim, and R. Armstrong, Phys. Rev. B **53**, 2425 (1996).
[22] Y. Tong, C. Rice, A. Wieckowski, and E. Oldfield, J. Am. Chem. Soc. **122**, 1123 (2000).
[23] D. J. Advena, V. T. Bly, and J. T. Cox, Appl. Opt. **32**, 1136 (1993).